Advancing ionospheric irregularity reconstruction with ICON/MIGHTI wind-driven insights

Tian, P. ORCID: https://orcid.org/0000-0001-8976-2711, Yu, B. ORCID: https://orcid.org/0000-0003-2758-1960, Xue, X. ORCID: https://orcid.org/0000-0002-4541-9900, Yamazaki, Y. ORCID: https://orcid.org/0000-0002-7624-4752, Owens, M. J. ORCID: https://orcid.org/0000-0003-2061-2453, Ye, H. ORCID: https://orcid.org/0000-0002-8371-9760, Wu, J. ORCID: https://orcid.org/0000-0002-3998-9296, Chen, T. ORCID: https://orcid.org/0000-0002-8399-4084, Scott, C. J. ORCID: https://orcid.org/0000-0001-6411-5649 and Dou, X. ORCID: https://orcid.org/0000-0001-6433-6222 (2025) Advancing ionospheric irregularity reconstruction with ICON/MIGHTI wind-driven insights. Geophysical Research Letters, 52 (12). e2025GL115666. ISSN 0094-8276 doi: 10.1029/2025GL115666 Available at https://centaur.reading.ac.uk/123269/

AGU ADVANCING EARTH AND SPACE SCIENCES

Geophysical Research Letters

RESEARCH LETTER
10.1029/2025GL115666

Advancing Ionospheric Irregularity Reconstruction With ICON/MIGHTI Wind-Driven Insights

Penghao Tian[1,2], Bingkun Yu[1,2,3], Xianghui Xue[1,2,4], Yosuke Yamazaki[5], Mathew J. Owens[6], Hailun Ye[1,2], Jianfei Wu[1,2], Tingdi Chen[1,2], Christopher J. Scott[6], and Xiankang Dou[1,2]

[1]School of Earth and Space Sciences, University of Science and Technology of China, Hefei, China, [2]CAS Key Laboratory of Geospace Environment, CAS Center for Excellence in Comparative Planetology, Anhui Mengcheng Geophysics National Observation and Research Station, University of Science and Technology of China, Hefei, China, [3]Institute of Deep Space Sciences, Deep Space Exploration Laboratory, Hefei, China, [4]Hefei National Laboratory, University of Science and Technology of China, Hefei, China, [5]Leibniz Institute of Atmospheric Physics at the University of Rostock, Kühlungsborn, Germany, [6]Department of Meteorology, University of Reading, Reading, UK

Key Points:

- The sporadic E layers observed by COSMIC-2 and neutral wind by ICON/Michelson Interferometer for Global High-resolution Thermospheric Imaging exhibit consistency in the Northern Hemisphere, explained by ion drift induced by wind shear
- A deep-learning model with neutral wind-driven for Es layer prediction has been developed based on wind shear theory and artificial intelligence techniques
- Incorporating wind shear mechanism prior knowledge significantly improved model performance, increasing the accuracy from 71.6% to 87.9%

Correspondence to:

B. Yu and X. Xue,
bkyu@ustc.edu.cn;
xuexh@ustc.edu.cn

Citation:

Tian, P., Yu, B., Xue, X., Yamazaki, Y., Owens, M. J., Ye, H., et al. (2025). Advancing ionospheric irregularity reconstruction with ICON/MIGHTI wind-driven insights. *Geophysical Research Letters*, *52*, e2025GL115666. https://doi.org/10.1029/2025GL115666

Received 1 MAR 2025
Accepted 23 MAY 2025

Abstract In the mesosphere-lower thermosphere region, atmospheric plasma components exhibit short-term enhancements, forming sporadic E (Es) layers that impact communication systems. The prevailing theory posits that neutral wind shear is the primary driver of mid-latitude Es layer. Here, we present neutral wind field data from the ICON/Michelson Interferometer for Global High-resolution Thermospheric Imaging mission during 2019–2022, revealing a clear relationship between wind shear and Es layer formation in the Northern Hemisphere. Notably, the vertical ion divergence/convergence significantly impact mid-latitude Es production. Inspired by deep learning techniques, we developed a deep learning model based on wind shear and neutral wind data, reconstructing the small-scale morphology of Es layers. Vertical ion convergence information derived from the wind shear physical equations was found to be a key factor in enhancing model performance. Our results demonstrate that incorporating physical data from vertical ion drift improves the predictive capabilities of ionospheric irregularities artificial intelligence models, increasing the accuracy from 71.6% to 87.9%.

Plain Language Summary In the region between Earth's mesosphere and lower thermosphere, thin layers of dense plasma, known as sporadic E (Es), can form suddenly and interfere with radio communications. These layers are influenced by wind patterns at their respective altitudes, but limited data has made it challenging to fully understand their formation and improve predictions. In this study, we used new satellite observations to investigate how high altitude winds contribute to Es layer formation. Inspired by the growing role of artificial intelligence (AI) in scientific breakthroughs, as recognized by the 2024 Nobel Prize in Physics, we developed an AI model that integrates wind patterns and physics-based equations to predict Es occurrences. Our results show that including information on ion movement, particularly how ions converge under wind shear effects, significantly enhances model accuracy. This approach offers new insights into how Es layers form and improves forecasting methods, helping to mitigate their impact on communication systems.

1. Introduction

Sporadic E (Es) layers are transient and dense ionospheric plasma layers typically observed at altitudes ranging between 90 and 120 km in the mesosphere-lower thermosphere (MLT) region (Vincent, 2015). Composed mainly of metallic ions such as Fe^+ and Mg^+ originating from meteoric ablation (Plane, 2003), these layers form thin sheets that can significantly impact radio wave propagation, particularly high-frequency (HF) and very high-frequency radio signals, often used in aircraft navigation and remote sensing applications (Haldoupis, 2011; Mathews, 1998). Characterizing Es layers, however, remains challenging due to their spatial and temporal variability, as they exhibit horizontal extents from 10 to 1,000 km and vertical thicknesses from 0.5 to 5 km (Whitehead, 1989; Yu et al., 2019). Observational techniques have advanced from early ground-based ionosondes and radars to in situ measurements and satellite-based radio occultation (RO), providing a broader perspective on Es layer distribution and behavior across different latitudes and seasonal variations (Gardner et al., 1993; Miller & Smith, 1978; Wickert et al., 2009; Yue et al., 2015; Zhao et al., 2024). However, despite extensive research, capturing the global distribution and understanding the complex dynamics of Es layers remains a pressing challenge in ionospheric forecasting.

The widely accepted theory for Es layer formation is the neutral wind shear mechanism, which posits that vertical shears in horizontal neutral winds drive the convergence of metallic ions, thereby forming thin, dense plasma layers at specific altitudes (Axford, 1963; Aylett et al., 2024; Haldoupis, 2011; Yamazaki et al., 2022; Yu, Xue, et al., 2021). Unlike other ionospheric layers, formed by the photo-ionization of N_2 and O_2, in which the major molecular ions NO^+ and O_2^+ have lifetimes on the order of seconds, the Es layer is composed of long-lived (up to 10 d) metallic ions (Plane et al., 2015) and is remarkably thin, typically 1–3 km thick (Layzer, 1972). This convergence of metallic ions, primarily through vertical gradients in the eastward wind, is theorized to lead to the formation of Es layers, particularly at mid-latitudes where such wind shears are common (Whitehead, 1961, 1970; Wu et al., 2019; Yu, Xue, et al., 2021). Under this theory, vertical ion velocities are influenced by the Lorentz force, with the zonal component of the neutral wind playing a dominant role in driving vertical ion convergence in the E region (Qiu et al., 2019).

Despite the foundational framework provided by wind shear theory, empirical evidence linking Es layer formation directly to neutral wind shear remains limited and, in some cases, inconsistent (Bishop et al., 2005; Kunduri et al., 2023; Larsen et al., 1998; Liu et al., 2018; Yamazaki et al., 2022). This presents a challenge for Es modeling, but artificial intelligence (AI) techniques offer a potential solution to address this issue. In recent years, deep learning techniques have gained remarkable recognition for their transformative impact across various scientific fields, highlighted by the 2024 Nobel Prize in Physics for advancements in AI (Gibney & Castelvecchi, 2024; Hopfield, 1982). These techniques have shown significant promise for atmospheric and ionospheric modeling, offering novel methods to interpret complex, high-level data. Examples include deep learning for the prediction of global Es patterns (Tian et al., 2022) or TEC distribution (Wang et al., 2023), ensemble learning using multi-source data fusing to improve ionospheric irregularity predictions (Tian et al., 2023) and estimating weak Es layers impact under different solar conditions using neutral networks (Tian et al., 2024), to name a few. However, these modeling approaches offer climatological models of the Es layer without considering the mechanisms influencing its formation (Yu et al., 2024). The primary challenge lies in the lack of observational data in the MLT region. Predicting the high-precision distribution of Es remains a challenging and unsolved problem.

In this study, we investigate the evolution of mid-latitude Es layers in the Northern Hemisphere by integrating COSMIC-2 and ICON/MIGHTI observations with AI-driven modeling. By incorporating neutral wind shear dynamics into deep learning models, we assess their role in reconstructing Es morphology and improving predictive accuracy. Comparisons between observational data and model results reveal how neutral wind shear influence the evolution and predictability of mid-latitude Es layers, providing a more reliable framework for space weather prediction.

Section 2 describes the data sets and modeling approaches used in this study. Section 3 presents a comparative analysis of Es layer structures derived from observations and model predictions. Section 4 summarizes the key findings and implications of this work.

2. Data and Methods

The Formosa Satellite-7/Constellation Observing System for Meteorology, Ionosphere, and Climate-2 (FORMOSAT-7/COSMIC-2) (Schreiner et al., 2020), a launched equatorial constellation of six satellites carrying advanced RO receivers, exhibits high signal-to-noise ratio (SNR) and the ability to provide high vertical resolution profiles of bending angles and refractivity, which contain information on the upper atmosphere and ionosphere (Anthes & Schreiner, 2019). By May 2021 the COSMIC-2 satellites have deployed into six evenly spaced circular orbital planes of 24° inclination at an altitude of about 550 km. Each satellite carries two space weather instruments, the Ion Velocity Meter and the Radio Frequency Beacon, which will contribute to the forecasting of space weather events, monitoring and prediction of scintillation (e.g., sporadic E layers). For this study, SNR data were used to calculate the maximum S4 scintillation index (S4max), which is indicative of ionospheric scintillation caused by Es layers. Following established methodologies (Tian et al., 2024), the valid S4 profiles from 80 to 130 km between 2019 and 2022 were calculated and the anomalous disturbance profiles unrelated to Es events were excluded.

The Michelson Interferometer for Global High-resolution Thermospheric Imaging (MIGHTI) instrument was built for launch and operation on the NASA Ionospheric Connection Explorer (ICON) mission (Englert

et al., 2017, 2023). MIGHTI measures horizontal wind velocities via Doppler shifts in airglow emissions at 557.7 nm, covering altitudes from 90 to 300 km with a vertical resolution of ∼3 km, during day and night. The version 5 of the cardinal wind profiles, which cover the latitude range between 12°S and 42°N, from the green-line emission from 2019 to 2022 were used. Only ICON/MIGHTI data with a "wind quality factor" of one, as described by Englert et al. (2023), were used in this study. This criterion ensures the use of the highest quality data and excludes measurements affected by radiation near the South Atlantic Anomaly, which can contaminate the MIGHTI detectors.

The valid S4max data at 80–130 km from COSMIC-2 covers the period from 2019 to 2024, with a total of 11,245,839 profiles. The valid Es events were identified by ensuring altitude coverage between 80 and 130 km with gaps less than 3 km, and extracting the maximum S4 index within this range as the representative scintillation intensity, that is, Es intensity (Yu et al., 2019). The ICON/MIGHTI neutral data spans from December 2019 to November 2022. For each valid Es event, data with the same spatiotemporal conditions (conjunction) were extracted, using a spatial grid criterion of less than 2.5° in both latitude and longitude and a temporal separation of less than 20 min. This selection criterion is aligned with previous studies (Yamazaki et al., 2022), ensuring a balance between maintaining high data quality and providing sufficient sample to meet the training requirements of deep learning models. Conjunctions are treated to be independent as long as the Es profiles are different. For multiple neutral wind field measurements corresponding to a single Es event, the average values were used for statistical reliability. Each valid Es conjunction event in the data set is a single profile. The analysis period, spanning from December 2019 to November 2022, covers a latitude range from 15°S to 45°N, resulting in a total of 36,089 conjunction events.

The ion drift velocity for each conjunction event can be calculated using wind shear theory. The wind shear mechanism, a foundational theory for Es layer formation, describes how vertical gradients in horizontal neutral winds lead to ion convergence. The steady-state ion momentum equation is $0 = e(\mathbf{v_{ion}} \times \mathbf{B} + \mathbf{E}) - Mv_{ion-neutral}(\mathbf{v_{ion}} - \mathbf{V_{neutral}})$, where M is the ion mass, $\mathbf{B} = B_0(\sin D \cos I, \cos D \cos I, -\sin I)$ is the magnetic field, I and D are the dip angle and declination angle of the magnetic field. We set $\mathbf{v_{ion}} = (\mathrm{u_{ion}}, \mathrm{v_{ion}}, \mathrm{w_{ion}})$ and $\mathbf{V_{neutral}} = (\mathrm{U}, \mathrm{V}, \mathrm{W})$ for the ion drift velocity and neutral wind. The vertical ion drift velocity $(\mathrm{w_{ion}})$ was calculated using the following equation (Yu, Xue, et al., 2021):

$$\mathrm{w_{ion}} = \frac{r\cos D\cos I - \sin D\sin I\cos I}{1+r^2}\mathrm{U} - \frac{r\sin D\cos I + \cos D\sin I\cos I}{1+r^2}\mathrm{V} + \frac{r^2+\sin^2 I}{1+r^2}\mathrm{W}; \quad r = \frac{v_{ion-neutral}}{\omega_{ci}}$$

where $v_{ion-neutral}$ is the ion-neutral collision frequency, $\omega_{ci} = eB_0/M$ is the ion gyrofrequency. The $v_{ion-neutral}$ is calculated from the empirical atmospheric model, NRLMSIS 2.0 (Emmert et al., 2021), which provides the neutral atmospheric densities (N_2, O_2 and O) by inputting parameters (time, altitude, latitude, longitude, F10.7 index, and Ap index) to determine ion-neutral collision frequency. The calculated vertical wind velocity is used to derive the vertical ion convergence term by computing its minus gradient, i.e., $\partial N/\partial z \sim -\partial \mathrm{w_{ion}}/\partial z|z = z_0$, where z_0 is the given altitude.

In our earlier work, we introduced Sporadic E Layer Forecast using Artificial Neural Networks (i.e., SELF-ANN), a deep learning framework, which is grounded in the principles of residual network architecture (Tian et al., 2023). The neutral wind-driven model in this study is based on SELF-ANN architecture, open source on tianph (2023). Algorithmically, a deep neural network learns the relationship between the manifolds representing the input data and labels (Islam et al., 2023). The model architecture is based on a residual neural network (ResNet) framework, featuring skip connections to ensure efficient gradient flow and robust learning of spatiotemporal dependencies. The trained model predicts the ionospheric scintillation index using two sets of input features: spatiotemporal parameters $\mathbf{S}^{input}$, which include local time, latitude, longitude, altitude, and day of year, and neutral wind-derived features $\mathbf{N}^{input}$, specifically the vertical ion convergence computed from the wind shear equation. The vertical ion convergence is calculated using horizontal wind profiles from ICON/MIGHTI observations, magnetic inclination, and declination from the International Geomagnetic Reference Field model,

and neutral atmospheric density from the NRLMSIS empirical model. The model architecture follows the SELF-ANN framework, consisting of stacked residual blocks incorporating convolutional layers (Conv1 × 1 and Conv3 × 3), batch normalization, and ReLU activations, enabling the network to effectively learn nonlinear mappings between physical inputs and ionospheric irregularities. See Tian et al. (2023) for more information about the input parameters. The model outputs scintillation values $\mathbf{D}^{pred}$, which are evaluated using various metrics, including mean absolute error (MAE), root mean square error (RMSE), and Spearman correlation.

3. Results

Figure 1 presents the relationship between COSMIC-2 observations of the Es layer intensity and the horizontal shear of the ICON/MIGHTI neutral wind data at 15°S–45°N at 80–130 km during December 2019–November 2022. Figures 1a and 1b show the global distribution of zonal wind shear (i.e., vertical shear of the zonal wind) and vertical ion divergence (i.e., vertical gradient in the vertical ion drift velocity) at 105 km, respectively. Figure 1c presents the distribution of mid-latitude Es layers from COSMIC-2, as indicated by the S4max index. In the upper three panels, the vertical ion divergence and vertical shear of the zonal wind exhibit similar patterns, which is attributed to the dominance of the zonal wind component in the wind shear equation, that is, $w_{ion} \sim (r \cos D \cos I - \sin D \sin I \cos I)\left(1 + r^2\right)\mathrm{U}$. The vertical shear of the zonal wind ranges from ±10 m/s/km, and the calculated global ion vertical divergence is within ±0.15 m/s/km. Near the magnetic equator, the vertical ion divergence induced by wind shear is maximal, that is, the vertical ion convergence is minimal. The intensity of Es in the summer hemisphere is higher than in the winter hemisphere, with the enhanced occurrence in the summer attributed to the seasonal dependence of metallic ion density and vertical wind shear. Moreover, the Es intensity is found to be negatively correlated with the vertical ion divergence. Next, we compared all the data from the COSMIC-2 and ICON/MIGHTI wind field conjunction observations, which include 36,089 conjunction events. The time range of these events spans from December 2019 to November 2022. Figures 1d–1f display the correlations between different wind-driven parameters at 105 km (vertical shear of the zonal wind, vertical shear of the meridional wind, and vertical ion divergence) and the Es intensity derived from COSMIC-2/ICON conjunction observations. The Es intensity are computed for every 0.3 m/s/km (blue dots) and 1 m/s/km (red dots) in the vertical shear of horizontal wind in Figures 1d and 1e. For the vertical ion divergence, the Es intensity are computed for every 0.01 m/s/km (blue dots) and 0.05 m/s/km (red dots) in Figure 1f. Specifically, a strong negative correlation ($R = -0.97$) between vertical shear of the zonal wind and Es intensity, while Figure 1e shows a weak positive correlation ($R = 0.14$) between meridional wind shear and Es, which is attributed to the dominance of the zonal wind component in the wind shear equation. These results confirm the findings of previous work by Yamazaki et al. (2022). In contrast, Figure 1f reveals a moderate negative correlation ($R = -0.79$) between vertical ion divergence and Es intensity. Es layers in these results conform well to expectations from the wind shear theory. Furthermore, we computed the zonal ion divergence and the meridional ion divergence, which are not included in the figure. Their correlations with Es intensity are −0.59 and 0.11, respectively, contributing less than the vertical ion divergence.

Figure 1g illustrates two distinct regions: the top section shows the spatial distribution of Es layers, with weak and strong Es regions marked, and the lower section highlights plasma vertical convergence as derived from ICON/MIGHTI neutral wind, showing areas of divergence and convergence linked to Es layer formation. According to the wind shear theory, since $r \gg 1$ below ∼115 km, U is more efficiently causing vertical plasma drift than V in the lower E region. Therefore, the term, $(r \sin D \cos I + \cos D \sin I \cos I)\left(1 + r^2\right)\mathrm{V}$, becomes small there, so that mainly the zonal wind U is responsible for the vertical ion drift. The dominance of zonal wind shear in mid-latitude Es formation arises from the Lorentz force's effect on vertical ion drift, as indicated by the $r \cos D \cos I$ term in wind shear equation. Under typical conditions (30°N, 30°E, 25 June 2020), zonal and meridional wind weights are approximately 0.032 and 0.003, respectively, implying that zonal winds contribute over 91% to ion convergence. This explains the stronger observed correlation between zonal wind shear and Es intensity. Ion accumulation, and thus the formation of Es, is expected at altitudes where the vertical gradient of the ion drift is negative, which coincides with the region of maximum negative vertical shear of the zonal wind, dU/dz. This illustration highlights the complex relationship between the vertical ion divergence and Es layer formation, providing insights into how ion convergence/divergence contribute to mid-latitude Es intensity variations.

As shown in Figure 1, the wind shear theory underscores the critical role of vertical ion convergence in Es formation. Consequently, we have incorporated this as a physical prior into the AI model. Two models were

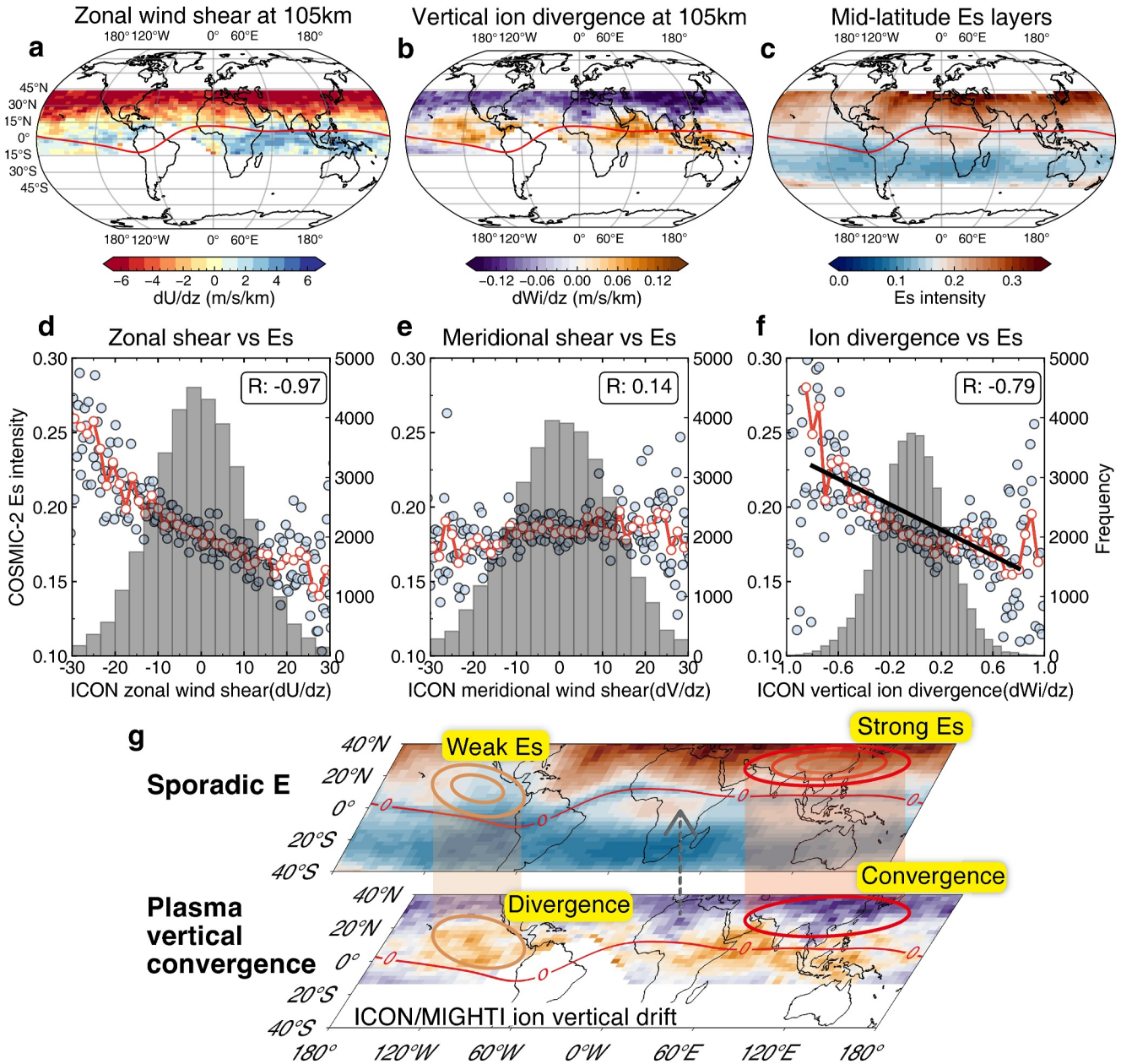

Figure 1. The wind shear mechanism of mid-latitude Es is validated using COSMIC-2 and ICON/Michelson Interferometer for Global High-resolution Thermospheric Imaging observations. Panels (a, b) show the zonal wind shear (i.e., vertical shear of the zonal wind) and vertical ion divergence (i.e., vertical gradient in the vertical ion drift velocity) at 105 km, respectively, with data from June to August, using neutral wind data with a quality factor of 1 and a grid resolution of 2.5 × 5°, excluding diurnal tidal effects. Panel (c) illustrates the mid-latitude Es layer distribution from 80 to 130 km observed by COSMIC-2 during June–August. Panels (d–f) show the distribution of zonal wind shear (i.e., vertical shear of the zonal wind), meridional wind shear (i.e., vertical shear of the meridional wind), and vertical ion divergence from the conjunction data at 15°S–45°N at 80–130 km during December 2019–November 2022, along with their relationship to Es intensity. The Es intensity (left *y*-axis) are computed for every 0.3 m/s/km (blue dots) and 1 m/s/km (red dots) in the vertical shear of horizontal wind (*x*-axis). Panel (g) demonstrates the correlation between vertical ion divergence and Es formation.

developed: a basic model, which predicts Es intensity solely based on spatiotemporal information without incorporating effective vertical ion convergence, and a neutral wind-driven model, which integrates vertical ion convergence derived from wind shear theory. The basic model serves as a reference for evaluating the added the physical information. The model accuracy was calculated by setting the occurrence threshold of 0.2 on the Es intensity. Figure 2 compares Es intensity from three sources: COSMIC-2/ICON conjunction observations, a basic model, and a neutral wind-driven model. The global distribution of the S4max index in the figure is similar to that

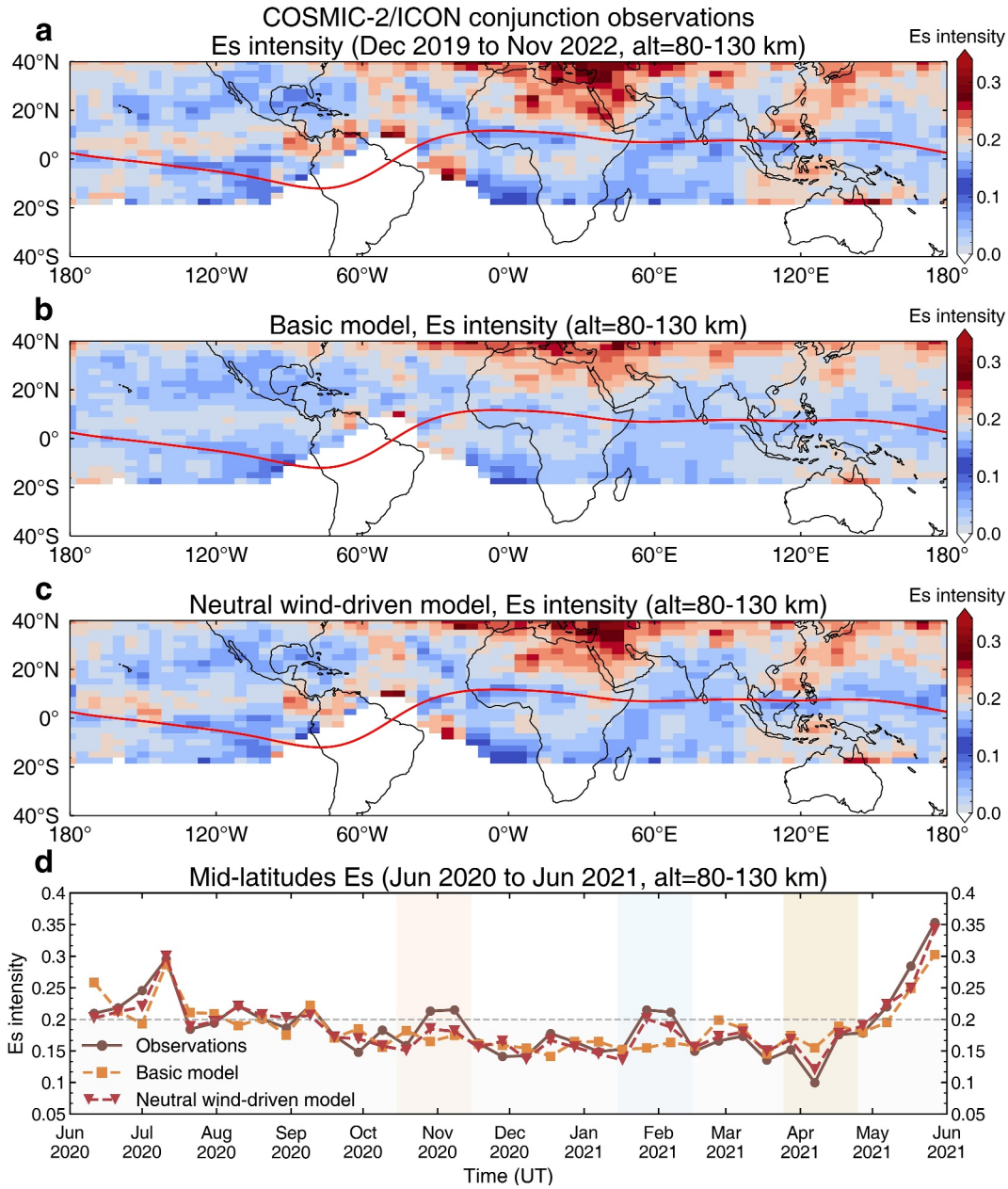

Figure 2. Comparison of observational data, the basic model, and the neutral wind-driven model results. Panel (a) shows the global distribution of Es from the conjunction observational data set. Panels (b, c) present the outputs from the basic model and the neutral wind-driven model, respectively. The magnetic equator was computed using the International Geomagnetic Reference Field. Panel (d) illustrates the mid-latitude Es variation from June 2020 to June 2021, with a statistical range from 20°N to 40°N. Different colored shading highlights the areas of model comparison. Compared to the basic model, the neutral wind-driven model incorporates effective vertical ion convergence.

in previous studies (Tian et al., 2023; Yu et al., 2019). The Es intensity is predominantly concentrated in the 20°N–40°N latitude range, where vertical ion convergence is significant.

Figure 2a shows the Es intensity observed between December 2019 and November 2022 at altitudes of 80–130 km, derived from COSMIC-2 and ICON conjunction data. Figure 2b presents the predictions from the basic model, and Figure 2c illustrates the predictions from the neutral wind-driven model for the same altitude range. A 2.5 × 5 degree sliding window was employed to calculate the average Es distribution. The basic model successfully reproduces the large-scale structure observed. In the mid-latitude region around 25°N, the basic model

fails to resolve small-scale fine structures, whereas the neutral wind-driven model produces results that are more consistent with observations. In Figure 2d, Es intensity data are averaged over 10-day intervals, focusing on the mid-latitude region between 20°N and 40°N. Notably, Es intensity peaks during June 2020 and June 2021, corresponding to the summer months in the Northern Hemisphere, but the values are weaker than in previous studies (Tian et al., 2023), likely due to reduced solar activity during this period. This seasonal increase is attributed to the enhanced vertical ion convergence observed in the mid-latitudes of the Northern Hemisphere, as illustrated in Figure 1. The intensity of Es increases in the red and blue shading areas, while it decreases in the yellow area, as indicated by the observations. The results of the neutral wind-driven model in these areas are more consistent with the observations. While the basic model successfully replicates the large-scale structure observed, it lacks the capability to capture small-scale details. In contrast, the neutral wind-driven model demonstrates a closer alignment with the observed spatial distribution, reflecting its improved ability to resolve small-scale features.

A more comprehensive evaluation of the neutral wind-driven model is presented in Figure 3. Figure 3a depicts the residual density distributions for both the basic and neutral wind-driven models. The basic model exhibits a broader Es intensity residual distribution spanning ±0.2, whereas the neutral wind-driven model is concentrated near zero, a trend further confirmed by the box plots. Next, we conduct a quantitative evaluation in both temporal and spatial domains. The seasonal distribution of Es layers and interhemispheric ion transport have demonstrated Es variability in response to solar radiation (Tian et al., 2023; Yu, Scott, et al., 2021). Figure 3b shows model results across four seasons. The left subpanel shows absolute error distributions, all below 0.1, while the right subpanel provides seasonal box plots with values concentrated within ±0.05. While both models effectively capture the climatological Es distribution, the neutral wind-driven model yields more precise outputs.

Figure 3c shows the spatial residual distribution for different latitude-longitude grid. The mid-latitude region (20°N–40°N) is divided into equally spaced 25 grid points, with Es intensity computed within each grid to characterize the geographic distribution. Overall, the neutral wind-driven model exhibits smaller deviations compared to the basic model, despite localized random discrepancies, indicating improved spatial accuracy across the mid-latitudes. Figure 3d presents the density distributions of Es intensity predicted by both models against observations. The square and triangular markers represent the basic and neutral wind-driven models, respectively, with marker points sampled from observational data. A linear fit to the basic model yields a slope of 0.31, indicating a negative bias, whereas the neutral wind-driven model achieves a slope of 0.8, much closer to the ideal value of 1, demonstrating improved agreement with observations.

Figure 3e evaluates the overall model performance. A random model, constructed via Gaussian kernel density estimation, serves as a reference by approximating the observed Es density distribution. The upper subpanel presents box plots of residuals and MAE across different altitudes (85, 95, 105, 115 km, and the broader 80–130 km range). The results obtained at different altitudes are consistent, with no significant differences observed. The lower subpanel shows the correlation coefficients for both models. Basic model has an MAE of ∼0.08 between observation and model outputs, which decreases to ∼0.05 when incorporating vertical ion convergence. The neutral wind-driven model effectively reconstructed the small-scale morphology of mid-latitude Es layers, yielding a MAE of 0.03 and RMSE of 0.08. Box plots show a narrower residual range, shifting from ±0.1 to near zero. The accuracy rate increased from 71.6% to 87.9%, and the spearman correlation coefficient also improves from 0.43 to 0.81. This analysis quantifies model performance across time, space, and altitude, highlighting the superior accuracy of the neutral wind-driven model and the critical role of vertical ion convergence in deep learning-based mid-latitude Es modeling.

Figure 4 illustrates the integration of wind shear theory into a deep learning framework for Es layer prediction. The top panel depicts the influence of wind shear in the MLT region. Vertical shear of the zonal wind, driven by opposing eastward and westward winds, induces ion convergence under the geomagnetic field, forming localized ion dense regions. While meridional winds can, in theory, drive ion motion along magnetic field lines, their influence on the wind shear mechanism is negligible. This is largely due to the suppression of vertical ion drift by polarization electric fields, which inhibits effective ion convergence and limits their role in Es layer formation. The middle panel presents the wind shear equation, formulated under the assumptions of steady-state conditions and rapid ion response times. Using this equation, vertical ion convergence are derived from ICON/MIGHTI wind field observations, geomagnetic field data from IGRF-13, and neutral atmospheric density from the NRLMSIS 2.0 empirical model. The approximate formula for ion-neutral collision frequency is

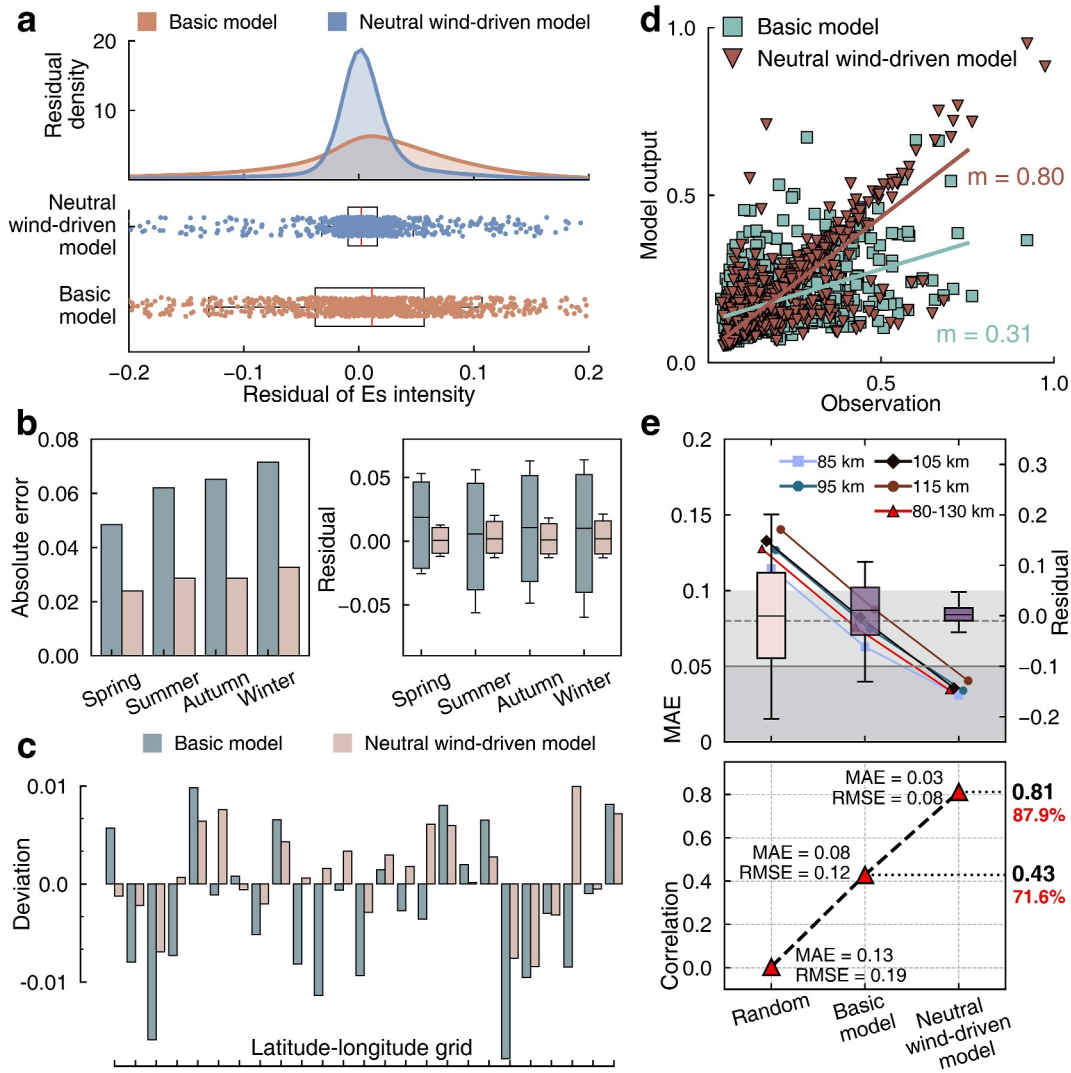

Figure 3. Validation of the basic Es model and neutral wind-driven Es model using COSMIC-2 observations. Panel (a) illustrates the residual distributions of the two models compared to observations. Panel (b) shows the deviation distributions for four seasons (spring, summer, autumn, and winter), with absolute error distributions on the left and box plots of residuals on the right. Panel (c) depicts the residual distributions across 50 geographic grids, covering the mid-latitude region between 20°N and 40°N. Panel (d) presents the density distributions and linear fit curves for the outputs of the two models compared to observational data. Panel (e) quantifies the performance of different models. The upper panel includes box plots of residuals and mean absolute error values across different altitudes, while the lower panel shows Spearman correlation coefficients. Data points in panels (a, d) are resampled from the data set. The random model in panel (e) uses a Gaussian kernel density estimation function, fitted to the density distribution of the observational data.

$\nu_{ion-neutral} = 2.6 \times 10^{-9} N_n / \sqrt{m_n}$, where N_n is neutral atmospheric number density and m_n denotes the mean neutral molecular mass (N_2, O_2, and O) in atomic mass units (Xue et al., 2013). As illustrated in Figure 1, vertical ion convergence plays a critical role in mid-latitude Es formation. The bottom panel shows the SELF-ANN based neutral wind-driven model framework. The model integrates neutral wind data with the Multi-Layer Perceptron architecture, which processes projected features using convolutional layers (Conv1 × 1, Conv3 × 3) and normalizations. By integrating ICON/MIGHTI neutral wind data and extracting key spatial features, the model learns the coupling between ion convergence patterns and Es formation, enabling accurate reconstruction of small-scale Es structures aligned with the dominant wind shear mechanism at mid-latitudes.

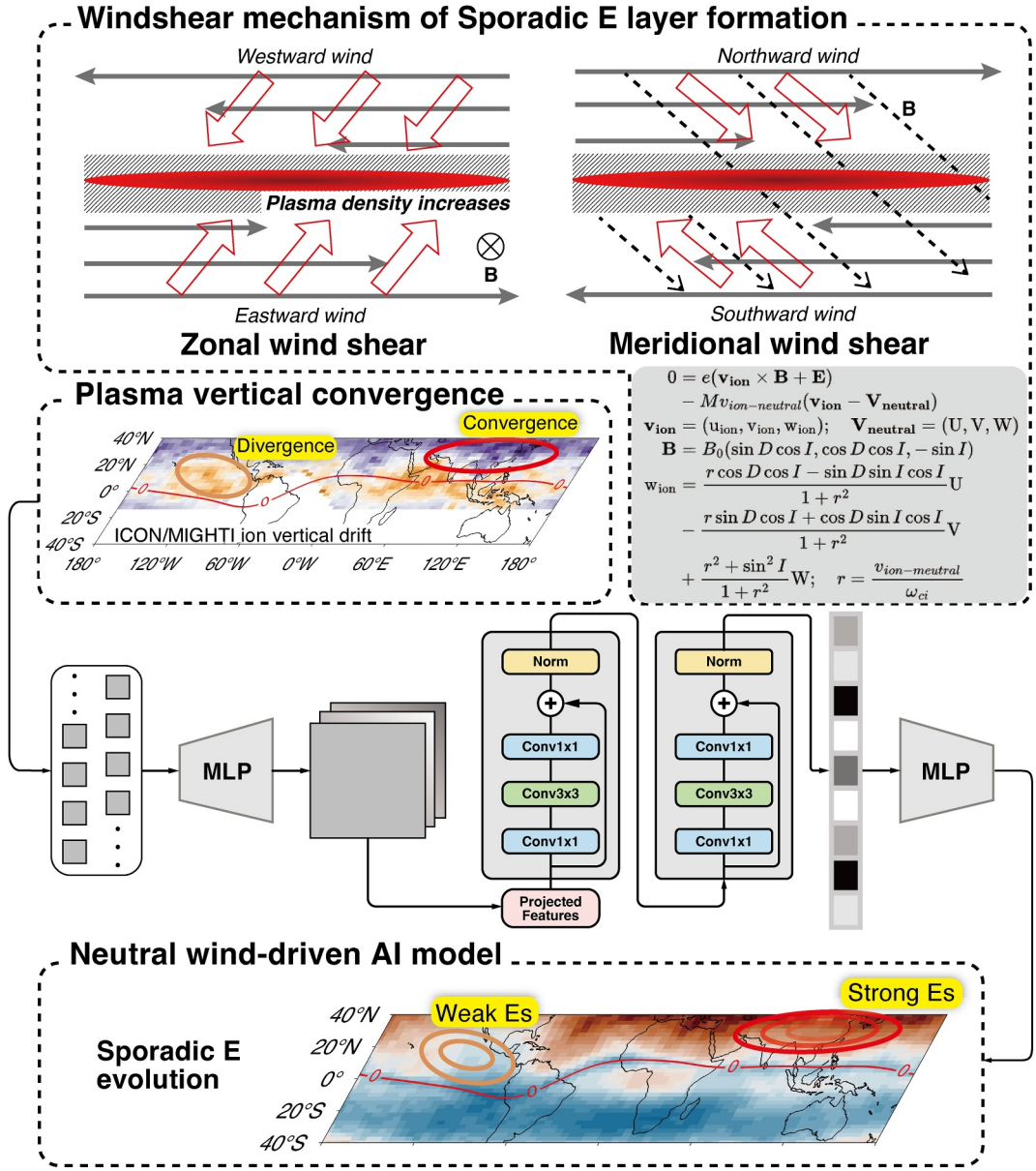

Figure 4. Schematic of the neutral wind-driven model. The top panel illustrates the wind shear mechanism for mid-latitude Es formation, with zonal and meridional wind dynamics in the geomagnetic field shown on the left and right, respectively. The middle panel presents the calculated vertical ion convergence distribution and formula involved. The bottom panel depicts the Sporadic E Layer Forecast using Artificial Neural Networks based model framework. Collision frequency (ion-neutral collision and ion gyrofrequency) is computed using magnetic field data from IGRF-13 and neutral atmospheric density from the NRLMSIS 2.0 empirical model.

4. Conclusions

The relationship between AI models for ionospheric irregularity prediction and wind shear mechanisms has not been thoroughly explored. This study proposes and validates an AI model driven by neutral wind shear for modeling and predicting the evolution of mid-latitude Es layers. By calculating the three-dimensional ion drift velocity based on wind shear theory, the results show that vertical ion divergence/convergence significantly impact mid-latitude Es intensity in the Northern Hemisphere, exceeding the influence of zonal and meridional ion convergence. Next, building on our previous AI models for Es prediction (Tian et al., 2023), we integrated vertical ion convergence data into the model and developed a neutral wind-driven Es model. The model effectively reconstructed the small-scale morphology of mid-latitude Es layers. Compared to the basic Es model without

effective vertical ion convergence information, the neutral wind-driven Es model significantly improved predictive accuracy, with the spearman correlation coefficient rising from 0.43 to 0.81 and the accuracy improving from 71.6% to 87.9%. Our results demonstrate that incorporating physical information from vertical ion drift markedly improves the predictive capabilities of ionospheric irregularities AI models. This work not only underscores the potential of deep learning-based techniques in ionospheric research but also advances the development of physics mechanism-driven methods in space weather modeling.

Data Availability Statement

The COSMIC-2 radio occultation data (podTc2 of level 1b, absolute total electron content profiles) are available from CDAAC: COSMIC Data Analysis and Archive Center: https://www.cosmic.ucar.edu/what-we-do/cosmic-2/data/. The ICON/MIGHTI Level 2.2 product Cardinal Vector Winds (Vector Wind Green Version 5) is accessible from the ICON website https://icon.ssl.berkeley.edu/Data. The source code of NRLMSIS 2.0 model can be downloaded from the website https://ccmc.gsfc.nasa.gov/models. The source code of SELF-ANN deep learning model is accessible in the github website: https://github.com/RuleNHao/SELF-ANN.

Acknowledgments

P. T. is grateful for the comments offered by Prof. John M. C. Plane (University of Leeds) and early training experiments implemented by Dr. Jingming Chen (Aerospace Information Research Institute, CAS) and Dr. Weiyu Hu (Peking University). This work was supported by the National Natural Science Foundation of China (42125402), the Project of Stable Support for Youth Team in Basic Research Field, CAS (YSBR-018), the National Natural Science Foundation of China (42188101 and 42374183), the Innovation Program for Quantum Science and Technology (2021ZD0300300), the National Natural Science Foundation of China (NSFC) Distinguished Overseas Young Talents Program, the Basic Research Project of the National Key Laboratory of Deep Space Exploration (NKLDSE2023A002), the Pre-research project on Civil Aerospace Technologies D010305 and D010301 funded by China National Space Administration (CNSA). XXH is grateful for the support from the New Cornerstone Science Foundation through the XPLORER PRIZE.

References

Anthes, R., & Schreiner, W. (2019). Six new satellites watch the atmosphere over Earth's equator. *Eos*, *100*. https://doi.org/10.1029/2019eo131779

Axford, W. (1963). The formation and vertical movement of dense ionized layers in the ionosphere due to neutral wind shears. *Journal of Geophysical Research*, *68*(3), 769–779. https://doi.org/10.1029/jz068i003p00769

Aylett, T., Feng, W., Marsh, D. R., Themens, D. R., & Plane, J. M. C. (2024). Characteristics of sporadic e layer occurrence in a global chemistry-climate model: A comparison with cosmic-derived data. *Authorea Preprints*.

Bishop, R., Earle, G., Larsen, M., Swenson, C., Carlson, C., Roddy, P., et al. (2005). Sequential observations of the local neutral wind field structure associated with E region plasma layers. *Journal of Geophysical Research*, *110*(A4), A04309. https://doi.org/10.1029/2004ja010686

Emmert, J. T., Drob, D. P., Picone, J. M., Siskind, D. E., Jones, M. Jr., Mlynczak, M. G., et al. (2021). NRLMSIS 2.0: A whole-atmosphere empirical model of temperature and neutral species densities. *Earth and Space Science*, *8*(3), e2020EA001321. https://doi.org/10.1029/2020ea001321

Englert, C. R., Harlander, J. M., Brown, C. M., Marr, K. D., Miller, I. J., Stump, J. E., et al. (2017). Michelson interferometer for global high-resolution thermospheric imaging (MIGHTI): Instrument design and calibration. *Space Science Reviews*, *212*(1–2), 553–584. https://doi.org/10.1007/s11214-017-0358-4

Englert, C. R., Harlander, J. M., Marr, K. D., Harding, B. J., Makela, J. J., Fae, T., et al. (2023). Michelson interferometer for global high-resolution thermospheric imaging (MIGHTI) on-orbit wind observations: Data analysis and instrument performance. *Space Science Reviews*, *219*(3), 27. https://doi.org/10.1007/s11214-023-00971-1

Gardner, C. S., Kane, T. J., Senft, D. C., Qian, J., & Papen, G. C. (1993). Simultaneous observations of sporadic E, Na, Fe, and Ca^+ layers at Urbana, Illinois: Three case studies. *Journal of Geophysical Research*, *98*(D9), 16865–16873. https://doi.org/10.1029/93jd01477

Gibney, E., & Castelvecchi, D. (2024). Physics Nobel scooped by machine-learning pioneers. *Nature*, *634*(8034), 523–524. https://doi.org/10.1038/d41586-024-03213-8

Haldoupis, C. (2011). A tutorial review on sporadic E layers. *Aeronomy of the Earth's Atmosphere and Ionosphere*, 381–394. https://doi.org/10.1007/978-94-007-0326-1_29

Hopfield, J. J. (1982). Neural networks and physical systems with emergent collective computational abilities. *Proceedings of the National Academy of Sciences of the United States of America*, *79*(8), 2554–2558. https://doi.org/10.1073/pnas.79.8.2554

Islam, M. T., Zhou, Z., Ren, H., Khuzani, M. B., Kapp, D., Zou, J., et al. (2023). Revealing hidden patterns in deep neural network feature space continuum via manifold learning. *Nature Communications*, *14*(1), 8506. https://doi.org/10.1038/s41467-023-43958-w

Kunduri, B. S. R., Erickson, P. J., Baker, J. B., Ruohoniemi, J. M., Galkin, I., & Sterne, K. (2023). Dynamics of mid-latitude Sporadic-E and its impact on HF propagation in the North American sector. *Journal of Geophysical Research: Space Physics*, *128*(9), e2023JA031455. https://doi.org/10.1029/2023ja031455

Larsen, M., Fukao, S., Yamamoto, M., Tsunoda, R., Igarashi, K., & Ono, T. (1998). The seek chemical release experiment: Observed neutral wind profile in a region of Sporadic E. *Geophysical Research Letters*, *25*(11), 1789–1792. https://doi.org/10.1029/98gl00986

Layzer, D. (1972). Theory of midlatitude Sporadic E. *Radio Science*, *7*(3), 385–395. https://doi.org/10.1029/rs007i003p00385

Liu, Y., Zhou, C., Tang, Q., Li, Z., Song, Y., Qing, H., et al. (2018). The seasonal distribution of Sporadic E layers observed from radio occultation measurements and its relation with wind shear measured by TIMED/TIDI. *Advances in Space Research*, *62*(2), 426–439. https://doi.org/10.1016/j.asr.2018.04.026

Mathews, J. (1998). Sporadic E: Current views and recent progress. *Journal of Atmospheric and Solar-Terrestrial Physics*, *60*(4), 413–435. https://doi.org/10.1016/s1364-6826(97)00043-6

Miller, K., & Smith, L. (1978). Incoherent scatter radar observations of irregular structure in mid-latitude Sporadic E layers. *Journal of Geophysical Research*, *83*(A8), 3761–3775. https://doi.org/10.1029/ja083ia08p03761

Plane, J. M. (2003). Atmospheric chemistry of meteoric metals. *Chemical Reviews*, *103*(12), 4963–4984. https://doi.org/10.1021/cr0205309

Plane, J. M., Feng, W., & Dawkins, E. C. (2015). The mesosphere and metals: Chemistry and changes. *Chemical Reviews*, *115*(10), 4497–4541. https://doi.org/10.1021/cr500501m

Qiu, L., Zuo, X., Yu, T., Sun, Y., & Qi, Y. (2019). Comparison of global morphologies of vertical ion convergence and Sporadic E occurrence rate. *Advances in Space Research*, *63*(11), 3606–3611. https://doi.org/10.1016/j.asr.2019.02.024

Schreiner, W. S., Weiss, J., Anthes, R. A., Braun, J., Chu, V., Fong, J., et al. (2020). Cosmic-2 radio occultation constellation: First results. *Geophysical Research Letters*, *47*(4), e2019GL086841. https://doi.org/10.1029/2019gl086841

Tian, P., Yu, B., Ye, H., Xue, X., Wu, J., & Chen, T. (2022). Estimation model of global ionospheric irregularities: An artificial intelligence approach. *Space Weather*, *20*(9), e2022SW003160. https://doi.org/10.1029/2022sw003160

Tian, P., Yu, B., Ye, H., Xue, X., Wu, J., & Chen, T. (2023). Ionospheric irregularity reconstruction using multisource data fusion via deep learning. *Atmospheric Chemistry and Physics*, *23*(20), 13413–13431. https://doi.org/10.5194/acp-23-13413-2023

Tian, P., Yu, B., Ye, H., Xue, X., Wu, J., & Chen, T. (2024). Deep learning insights into ionospheric sporadic e irregularities under different solar activity conditions. *Journal of Geophysical Research: Machine Learning and Computation*, *1*(4), e2024JH000279. https://doi.org/10.1029/2024jh000279

tianph. (2023). Rulenhao/self-ann: Self-ann v1.0.0-alpha. *Zenodo*. https://doi.org/10.5281/zenodo.10016010

Vincent, R. A. (2015). The dynamics of the mesosphere and lower thermosphere: A brief review. *Progress in Earth and Planetary Science*, *2*, 1–13. https://doi.org/10.1186/s40645-015-0035-8

Wang, Z., Zou, S., Sun, H., & Chen, Y. (2023). Forecast global ionospheric tec: Apply modified u-net on vista tec data set. *Space Weather*, *21*(8), e2023SW003494. https://doi.org/10.1029/2023sw003494

Whitehead, J. (1961). The formation of the Sporadic-E layer in the temperate zones. *Journal of Atmospheric and Terrestrial Physics*, *20*(1), 49–58. https://doi.org/10.1016/0021-9169(61)90097-6

Whitehead, J. (1970). Production and prediction of Sporadic E. *Reviews of Geophysics (1985)*, *8*(1), 65–144. https://doi.org/10.1029/rg008i001p00065

Whitehead, J. (1989). Recent work on mid-latitude and equatorial Sporadic-E. *Journal of Atmospheric and Terrestrial Physics*, *51*(5), 401–424. https://doi.org/10.1016/0021-9169(89)90122-0

Wickert, J., Michalak, G., Schmidt, T., Beyerle, G., Cheng, C.-Z., Healy, S. B., et al. (2009). GPS radio occultation: Results from champ, grace and FORMOSAT-3/COSMIC. *Terrestrial, Atmospheric and Oceanic Sciences*, *20*(1), 35–50. https://doi.org/10.3319/tao.2007.12.26.01(f3c)

Wu, J., Feng, W., Xue, X., Marsh, D., Plane, J., & Dou, X. (2019). The 27-day solar rotational cycle response in the mesospheric metal layers at low latitudes. *Geophysical Research Letters*, *46*(13), 7199–7206. https://doi.org/10.1029/2019gl083888

Xue, X., Dou, X., Lei, J., Chen, J., Ding, Z., Li, T., et al. (2013). Lower thermospheric-enhanced sodium layers observed at low latitude and possible formation: Case studies. *Journal of Geophysical Research: Space Physics*, *118*(5), 2409–2418. https://doi.org/10.1002/jgra.50200

Yamazaki, Y., Arras, C., Andoh, S., Miyoshi, Y., Shinagawa, H., Harding, B., et al. (2022). Examining the wind shear theory of sporadic e with ICON/MIGHTI winds and COSMIC-2 radio occultation data. *Geophysical Research Letters*, *49*(1), e2021GL096202. https://doi.org/10.1029/2021gl096202

Yu, B., Scott, C. J., Xue, X., Yue, X., Chi, Y., Dou, X., & Lockwood, M. (2021). A signature of 27 day solar rotation in the concentration of metallic ions within the terrestrial ionosphere. *The Astrophysical Journal*, *916*(2), 106. https://doi.org/10.3847/1538-4357/ac0886

Yu, B., Tian, P., Xue, X., Scott, C. J., Ye, H., Wu, J., et al. (2024). Comparative analysis of empirical and deep learning models for ionospheric Sporadic E layer prediction. *Earth and Planetary Physics*, *9*(1), 10–19. https://doi.org/10.26464/epp2024048

Yu, B., Xue, X., Scott, C. J., Wu, J., Yue, X., Feng, W., et al. (2021). Interhemispheric transport of metallic ions within ionospheric Sporadic E layers by the lower thermospheric meridional circulation. *Atmospheric Chemistry and Physics*, *21*(5), 4219–4230. https://doi.org/10.5194/acp-21-4219-2021

Yu, B., Xue, X., Yue, X., Yang, C., Yu, C., Dou, X., et al. (2019). The global climatology of the intensity of the ionospheric Sporadic E layer. *Atmospheric Chemistry and Physics*, *19*(6), 4139–4151. https://doi.org/10.5194/acp-19-4139-2019

Yue, X., Schreiner, W., Zeng, Z., Kuo, Y.-H., & Xue, X. (2015). Case study on complex Sporadic E layers observed by GPS radio occultations. *Atmospheric Measurement Techniques*, *8*(1), 225–236. https://doi.org/10.5194/amt-8-225-2015

Zhao, H.-S., Xu, Z.-W., Xue, K., Wu, J., Liu, Y.-X., Feng, J., et al. (2024). Probable controls from the lower layers on Sporadic E layer over east Asia. *Journal of Geophysical Research: Space Physics*, *129*(7), e2023JA032379. https://doi.org/10.1029/2023ja032379